# Structural reliability based energy-efficient arctic position mooring control of moored offshore structures under ice loads

Xiaoyue Zhang, Yuanhui Wang, Ahmed Chemori

# Structural Reliability Based Energy-Efficient Arctic Position Mooring Control of Moored Offshore Structures Under Ice Loads*

Xiaoyue Zhang[a], Yuanhui Wang[a,*] and Ahmed Chemori[a,b]

[a]College of Intelligent Systems Science and Engineering, Harbin Engineering University, Nantong Street 145, Harbin, 150001, China
[b]LIRMM, University of Montpellier, CNRS, Montpellier, 34095, France

ARTICLE INFO

*Keywords*:
Arctic Position Mooring Control
Adaptive Fuzzy Dynamic Surface Control
Structural Reliability
Setpoint Chasing
Ice-load Disturbance Observer

ABSTRACT

This work develops an energy-efficient robust control for arctic position mooring systems subject to discontinuous ice loads and system uncertainties. To provide a safe and energy-efficient reference position for moored offshore structures, an improved structural reliability-based setpoint chasing algorithm is proposed. An ice-load disturbance observer is constructed to handle the arctic environmental disturbances, relaxes the continuity, differentiability, and boundedness requirements of disturbances. The system uncertainties are addressed by an adaptive fuzzy estimator. With the reference position and disturbance estimation, an improved dynamic surface control law is derived by introducing a novel filter to improve the convergence rate of the filter error, it enhances also the control performance of the arctic position mooring with fast response. Theoretical analysis proves the stability of the resulting closed-loop system and the boundedness of all its signals with the invariant set mechanism and Lyapunov theory. Comparative numerical simulations are carried out on a turret-moored floating production storage and offloading (FPSO) vessel to demonstrate the performance and effectiveness of the proposed control scheme.

## 1. Introduction

The arctic area is rich in oil and gas resources, accounting for 13% of the world's unproved reserves, and 30% of the world's total reserves, respectively. Due to the increasing energy demand, it has become an attractive resource development area (Gautier, Bird, Charpentier, Grantz, Houseknecht, Klett, Moore, Pitman, Schenk, Schuenemeyer et al., 2009). However, many arctic exploration areas are located in deep waters with harsh environmental conditions and heavy ice loads. The offshore structures, relying only on a mooring system or a dynamic positioning system, can no longer meet the needs of safe and economic development of arctic resources (Li, 2012). The position mooring system exploits the capacity of mooring cables to reduce vessel energy consumption and adopts the dynamic positioning system to improve cable safety (Skjetne and Ren, 2020). It provides an effective solution for arctic exploration from both safety and energy efficiency perspectives (Sangsoo and Kim, 2003).

Arctic position mooring control is often exposed to harsh arctic environments, including wind, waves, currents, and especially sea ice (Rahimi, Rausand and Wu, 2011), which is the main load affecting ship maneuvering and safety (Wu, Kong, Tang, Lei and Ji, 2021). Ice load rejection thereby is a key objective for the arctic position mooring. In Zhou, Su, Riska and Moan (2011), a numerical model is extended based on Su, Riska and Moan (2010) to evaluate the continuous ice load acting on a moored ship, ignoring wind, wave and current disturbances. Kjerstad and Skjetne (2014) adopted a configurable high-fidelity numerical model to develop a dynamic positioning framework while considering complex environmental disturbances in the managed ice . As an effective solution for handling disturbances, the observer is applied to handle ice loads. Jayasiri, Nandan, Imtiaz, Spencer, Islam and Ahmed (2017) developed an unscented Kalman filter-based observer to estimate both the vessel state and the ice load for dynamic positioning vessels in ice. Zhou, Moan, Riska and Su (2013) proposed an ice simulator interconnecting ship and ice dynamics. However, all the above disturbance rejectiom methods, as well as commonly used observers, including nonlinear passive observers (Fossen and Strand, 1999), high gain observers (Ngongi and Du, 2014), finite time observers (Xia, Liu, Zhao, Chen and Shao, 2019), etc., are all constructed based on the restrictive assumptions of continuity, differentiability and boundedness of disturbances. But ice loads may have a rapid variation and discontinuous interaction phenomenon, such as intermittent ice crushing, especially in low-speed oil exploitation operations (Mååttånen and Kårnå, 2011). Accordingly, these assumptions are not appropriate for arctic applications, as such external disturbances may lead to an unstable closed-loop system. Therefore, disturbance rejection considering the discontinuous and unsmooth behavior of ice loads is a key issue to be addressed in arctic position mooring control.

On account of the long-term offshore operations of ships in the harsh arctic environment, safety and energy efficiency are two issues to be solved for arctic position mooring control. Some studies have been proposed to solve the above issues. Kjerstad, Værnø and Skjetne (2016) proposed an improved pseudo-derivative feedback dynamic positioning

*This work is the result of the research project funded by the National Natural Science Foundation of China under Grant No.51879049, and the Natural Science Foundation of Heilongjiang Province under Grant No.LH2019E039.

*Corresponding author
zhangxiaoyue912@126.com (X. Zhang); wangyuanhui@hrbeu.edu.cn (Y. Wang); Ahmed.Chemori@lirmm.fr (A. Chemori)
ORCID(s): 0000-0003-2784-5778 (X. Zhang); 0000-0002-4951-7997 (Y. Wang); 0000-0001-9739-9473 (A. Chemori)

control law to provide highly reactive system responses, especially for ship-ice interaction applications. To directly compensate environmental disturbances and system uncertainties, an acceleration-based feedforward controller is proposed for arctic dynamic positioning (Kjerstad, Skjetne and Jenssen, 2011). In Jayasiri, Nandan, Imtiaz, Spencer and Ahmed (2016), a nonlinear model predictive controller is proposed to generate online optimal commands for arctic dynamic positioning considering both the actuator and state constraints. Considering energy consumption, Kang, Lee, Lim, Lee, Jang, Jung and Lee (2021) evaluated the improvement of the positioning performance in ice conditions by heading control. Besides, Lee, Choi, Lee and Jung (2019) proposed to introduce tension into optimal heading control to quickly determine the target heading and thus reduce the ice loads acting on the vessels. Indeed, the aforementioned position mooring systems excessively rely on thrusters, but conservatively exploit the capacity of the mooring system to maneuver the vessel position and heading. Consequently, it does not completely address the energy efficiency issue.

To achieve energy-efficient position mooring control, Wang, Tuo, Yang, Biglarbegian and Fu (2018) and Tuo, Wang, Yang, Biglarbegian and Fu (2018) introduced structural reliability as a quantitative security index to make full use of the mooring system with a guaranteed safety. Nevertheless, it is insufficient to reduce the control effort to take into account only one critical cable with minimal structural reliability. Considering all mooring cables, a setpoint chasing algorithm is proposed to minimize thruster usage and maximize the utilization of the mooring system (Skjetne and Ren, 2020). Nguyen and Sørensen (2009a,b) proposed the setpoint chasing algorithm in the form of a low-frequency filter to compensate for the mean environmental load. The setpoint is calculated offline by switching with the predetermined sea condition level. Fang, Blanke and Leira (2010) enhanced the algorithm with the mooring tension-based objective function, considering all mooring cables, to calculate the optimal setpoints online without environment classification. To better capture the dynamic effects and the safety of the mooring system, the structural reliability index is further introduced into the objective function as a weighting factor or in place of the tension term (Fang et al., 2010; Fang, Leira and Blanke, 2013). Recent research on setpoint-chasing algorithms further validates the effectiveness of the aforementioned approach (Fang, Blanke and Leira, 2015; Wang, Yang, He, Xu and Su, 2016; Bjørnø, Heyn, Skjetne, Dahl and Frederich, 2017; Xia et al., 2019). Nevertheless, all the above forms of objective functions neglect tension and reliability constraints, which can cause them to exceed their admission limits, and even lead to cable failure and safety issues in the worst cases. In addition, intelligent algorithms like the deep deterministic policy gradient approach (Yu, Wang, Li and He, 2020) and Q-learning techniques (He, Wang, Wang, Li and Xu, 2021) are also applied to setpoint chasing algorithms, but unlike the above methods, this is a model-free, off-policy approach that trains reinforcement learning agents with rewards obtained by interacting with the position mooring system to obtain the optimal setpoints. As a result, it is computationally complex, time-consuming, and has poor real-time performance. In conclusion, in order to provide energy-efficient and safe reference setpoints for position mooring systems in real time, we concentrate on solving the problems of objective function based setpoint chasing algorithms to improve the safety of mooring systems.

Inspired by the above studies, we propose to focus on safe and energy-efficient arctic position mooring control for moored offshore structures in the presence of ice loads, unknown time-varying environmental disturbances, and system uncertainties. The main contributions of the present work include:

1. An ice-load disturbance observer is proposed for arctic disturbances. Compared with existing disturbance rejection methods for position mooring systems, the proposed disturbance observer relaxes the constraints on continuity, boundedness, and differentiability of disturbances. It is the first time to address the harsh environmental disturbance with discontinuous ice loads in arctic position mooring control.
2. An improved setpoint chasing algorithm is proposed to obtain optimal reference positions for the arctic position mooring system. The improved algorithm introduces structural reliability constraints into the objective function to meet safety and energy consumption requirements. Compared with the conventional algorithm (Fang et al., 2013), the proposed one provides higher safety for all cables of the mooring system.
3. An adaptive fuzzy dynamic surface controller with disturbance compensation and optimal reference position is proposed. A novel filter is introduced into the dynamic surface controller to provide fast convergence, and an adaptive fuzzy estimator is employed to handle the system uncertainties. The proposed controller addresses both crucial issues of safety and energy efficiency, and achieves robust arctic position mooring control with a fast response and arbitrarily small errors.

The remainder of this paper is organized as follows. The problem formulation is described in Section 2. The control scheme design as well as the theoretical analysis of the system stability are discussed in Section 3. Comparative numerical simulations are conducted to demonstrate the effectiveness of the proposed control scheme in Section 4. The paper ends with some concluding remarks in Section 5.

## 2. Problem formulation

A turret-moored fully actuated surface vessel exposed to wind, waves, currents, and ice is considered. The vessel is moored through the mooring system, with symmetrically distributed cables connected to the vessel's turret and fixed on the seabed by anchors (eg. illustration of Fig.1). Since wave-frequency motion should not enter the feedback loop, only low-frequency motion should be considered in the

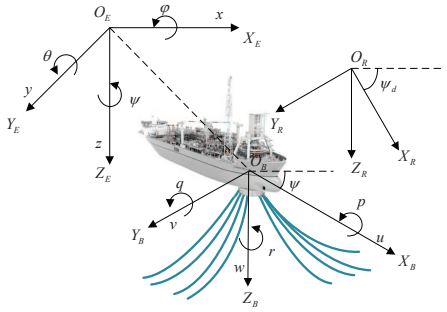


**Figure 1:** Illustration of a turret-moored surface vessel.

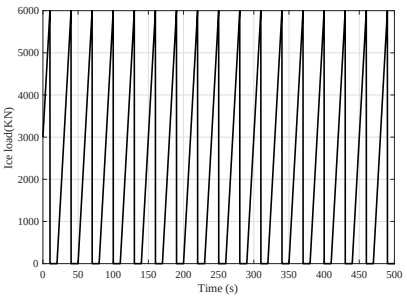


**Figure 2:** Simulated managed drifting ice loads.

controller design (Fossen, 1994), in which a three-degree-of-freedom (surge, sway, yaw) low-frequency model is adopted to design the position mooring control scheme. The proposed scheme should achieve energy efficient and safety, avoiding excessive control efforts for wave-frequency motions.

## 2.1. Kinematics and kinetics

A three-degree-of-freedom low-frequency motion kinematics and kinetics model of a moored vessel can be described as follows (Fossen, Thor I., 2002).

$$\dot{\eta} = J(\eta)\nu \tag{1}$$

$$M\dot{\nu} + C(\nu)\nu + D(\nu)\nu + \Delta = \tau + \tau_{env} + \tau_m \tag{2}$$

where $\eta = [x, y, \psi]^{\mathrm{T}}$ denotes the position and heading of the vessel in the earth-fixed coordinate frame $O_E X_E Y_E Z_E$, $\nu = [u, v, r]^{\mathrm{T}}$ denotes the velocity vector in the body-fixed frame $O_B X_B Y_B Z_B$. $M$ represents the system inertia matrix, $C(\nu)$ represents the Coriolis matrix, $D(\nu)$ represents damping matrices. $\Delta$ is the model uncertainty term, including parameter uncertainty and unmodeled dynamics, etc. $\tau = \left[\tau_X, \tau_Y, \tau_N\right]^{\mathrm{T}}$ denotes the control efforts produced by thrusters, $\tau_{env}$ represents the unknown environmental disturbances related to wind, waves, currents and ice, $\tau_m$ is the mooring force. $J(\eta)$ is the rotation matrix satisfying $\|J(\eta)\| = 1$ and $J(\eta)^{\mathrm{T}} J(\eta) = I_{3\times 3}$, defined as

$$J(\eta) = \begin{bmatrix} \cos(\psi) & -\sin(\psi) & 0 \\ \sin(\psi) & \cos(\psi) & 0 \\ 0 & 0 & 1 \end{bmatrix} \tag{3}$$

We consider a mooring system with $k$ cables, $T_i = \left[T_X^i, T_Y^i, 0\right]^{\mathrm{T}}$ is the contact force vector of the $i$th cable, where $T_i = T_i\left(\left\|p(t) - p_i\right\|\right) \triangleq \left\|T_i(\eta)\right\|$, $p = [x, y]^{\mathrm{T}}$ and $p_i = \left[x^i, y^i\right]^{\mathrm{T}}$ are the positions of the vessel and the $i$th anchor. The mooring force exerted on the vessel can then be expressed by low-frequency tension because the system uncertainty has taken into account the cable dynamics.

$$\tau_m = \left[\sum_{i=1}^{k} T_X^i, \sum_{i=1}^{k} T_Y^i, 0\right]^{\mathrm{T}} \tag{4}$$

**Assumption 1.** *Considering the nonlinear model (2) with the unknown system matrix $M$, $C(\nu)$, and $D(\nu)$, the model uncertainties can be described as $\Delta = \Delta M + \Delta C(\nu) + \Delta D(\nu)$. And the system uncertainties, include the model uncertainties and unknown system nonlinear terms, is modeled as $f = -C(\nu) - D(\nu) - \Delta$.*

**Remark 1.** All terms, including $C(\nu)$, $D(\nu)$, and environmental disturbances $\tau_{env}$ are time-varying implicitly obtained unknown terms, and are affected by the environment and ship motion. However, the noise will inevitably exist in position and velocity measurements of ship. Hence, it makes sense to assume that the model uncertainties $\Delta$ is related to the system matrix. Assumption 1 is reasonable.

## 2.2. Arctic ice loads

Due to the high energy and time-varying nonlinear characteristics of sea ice behavior, unmanaged drifting ice can generate long-term extreme ice loads that threaten vessel safety (Sinsabvarodom, Leira, Chai and Næss, 2021). For arctic offshore production operations, ice loads can only be reduced to a tolerable level by breaking large pieces of drifting ice into smaller and manageable fractions by icebreakers. Therefore, the arctic ice loads should be considered as managed ice, which can be described as a sequence of impulses exerted on the vessel, mixed with relatively long periods of ice-free load, as illustrated by the curve of Fig.2 (Daley, Alawneh, Peters, Quinton and Colbourne, 2012). It has a rapid decay rate during the unloading phase (Mååttånen and Kårnå, 2011). The ice loads have a discontinuous and non-smooth behavior, with a rapid change rate.

**Assumption 2.** *The arctic environmental disturbances induced by wind, waves, currents, and ice can be described as*

$$\tau_{env} = d + \sigma \tag{5}$$

*where $d$ is a smooth function with $\|\dot{d}\| < D(t)$ and $\|\sigma\| \leq \sigma^*$. $D(t)$ and $\sigma^*$ are a continuous function and an unknown positive constant, respectively.*

**Remark 2.** Arctic environmental disturbances $\tau_{env}$ include ice loads $\tau_{ice}$ and wind, wave and current disturbances $\tau_d$.

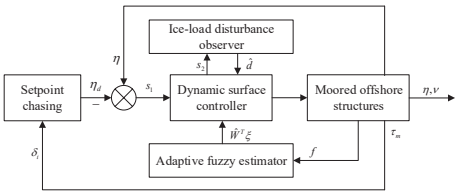


**Figure 3:** Block diagram of the proposed arctic position mooring.

It is discontinuous and non-differentiable due to the non-smooth ice load behavior. Such disturbance can be decomposed as (5), with the continuous part denoted by the smooth function $d$, and $\sigma$ represents the remaining discontinuous part.

Moreover, the non-smooth characteristics of the system uncertainty can also be included in the above disturbances. Disturbance as in Assumption 2 such that its derivative $\dot{d}$ exists satisfying $\|\dot{d}\| < D(t)$, releases the requirement that the disturbance should be discontinuous and differentiable. However, prior knowledge that the disturbance and its derivative are bounded requires further observer design to resolve.

### 2.3. Structural reliability index

To balance the demand for energy saving and mooring system security, Madsen, Krenk and Lind (2006) introduced the structural reliability index as a quantitative safety criterion to describe the possibility of cable breakage.

$$\delta_i = \frac{T_{b,i} - T_{exi}}{\sigma_{b,i}} = \frac{T_{b,i} - k_\sigma \sigma_i - T_i}{\sigma_{b,i}} \quad i = 1, \cdots, k \tag{6}$$

where $T_{b,i}$ is the average breaking strength of the $i$th cable, $k_\sigma$ is a scaling factor, $\sigma_i = 7.5\% T_i$ is the standard deviation of the time-varying mooring force, $T_i$ is the low frequency mooring force, and $\sigma_{b,i} = 7.5\% T_{b,i}$ is the standard deviation of the average breaking strength.

$\sigma_i$ includes high-frequency mooring forces, a slowly varying measure describing the sea state, which does not induce the wave-frequency motion of the vessel. So structure reliability is introduced considering the dynamic effects of mooring tension fluctuations. It will decrease with increasing mooring tension, while the cable breakage probability will increase.

## 3. Safe and energy efficient position mooring control scheme design

The main control objective is to design a safe and energy-efficient control scheme for arctic position mooring that maneuvers the vessel toward a setpoint where the mooring system is fully and safely used, while addressing discontinuous environmental disturbances and system uncertainties. The block diagram of the proposed arctic position mooring system is depicted in Fig.3.

### 3.1. Improved setpoint chasing algorithm

We improve the setpoint chasing algorithm by introducing structural reliability constraints into the objective function as follows

$$f\left(\delta_e^i\right) = \sum_{i=1}^{k} a_i \delta_e^{i\,2} = \sum_{i=1}^{k} a_i \left(\delta_i - \delta_d^i\right)^2 \quad \left(\delta_i > \delta_d^i\right) \tag{7}$$

where $a_i$ is the weighting factor, and $\delta_d^i$ is the desired structural reliability.

This objective function enables the structural reliability index of each cable as close as feasible to the desired value, so that the full capability of the mooring system can be utilized. And the reliability constraints $\delta_i > \delta_d^i$ are introduced to ensure that the structural reliability is greater than the desired value to avoid cable breakage and guarantee the safety of the mooring system. Note that the structural reliability accounts for the dynamic effect of the tension to offer a more conservative solution than the tension-based objective function.

It is evident from (4) and (6) that the tension and the vessel's position are related to structural reliability. By minimizing the reliability-based objective function (7) while satisfying the constraints, the optimal operating position can be determined. To get the optimal position increment, the mooring tension is expressed in terms of the vessel's horizontal motion (Strand, Sørensen and Fossen, 1998).

$$\begin{aligned} T_i &= T_{oi} + c_i \Delta d \\ &= T_{oi} - c_i \Delta r \sin\left(\beta + \beta_o^i\right) \end{aligned} \tag{8}$$

where $T_i$ and $T_{oi}$ are the mooring forces at the current and initial positions, respectively. $\Delta d$ is the change in horizontal distance between the ship and the anchor. $c_i$ denotes the incremental stiffness tension (Faltinsen, 1990). The changes in ship position and heading are indicated by $\Delta r$ and $\beta$, respectively.

The structural reliability-based objective function is connected to the vessel's position increment and heading by substituting (6) and (8) into (7). The constrained multivariable function solver is then used to determine the best solution for the minimization objective function, as well as the optimal position increment and heading for the vessel. The reference setpoints can be derived from the initial position.

$$\eta_s = \eta_o + \Delta r \begin{bmatrix} \cos\beta & \sin\beta & 0 \end{bmatrix}^{\mathrm{T}} \tag{9}$$

To generate a smooth path passing through the setpoints, a reference model is designed as follows (Sørensen, 2005)

$$\begin{aligned} \dot{\eta}_{ref} &= -\Lambda \eta_{ref} + \Lambda \eta_s \\ \dot{\eta}_d &= \nu_d \\ \dot{\nu}_d &= -\lambda_1 \eta_d - \lambda_2 \nu_d + \lambda_1 \eta_{ref} \end{aligned} \tag{10}$$

where $\eta_{ref}$ is the low-pass signal of the setpoints $\eta_s$, and $\Lambda$ is a diagonal gain matrix. $\eta_d$ and $\nu_d$ represent the desired position and velocity, respectively. The design parameters $\lambda_1$ and $\lambda_2$ are the diagonal stiffness matrix and the nonnegative diagonal damping matrix.

### 3.2. Adaptive fuzzy dynamic surface control

**Lemma 1.** *(Wang, 1999) For any real continuous function $f(x) \in U$ ($U \subset R^n$) and any arbitrary $\varepsilon^* > 0$, there exists a fuzzy system $\hat{f}(x)$ such that:*

$$\sup_{x \in U} \left| f(x) - \hat{f}(x) \right| \leq \varepsilon^* \tag{11}$$

Lemma 1 states that a fuzzy system can approximate any real continuous function $f(x) \in U$ with an arbitrary accuracy. Hence, we construct an adaptive fuzzy estimator to estimate the continuous unknown system uncertainties.

$$f\left(\underline{x}\right) = W^{\mathrm{T}} \xi\left(\underline{x}\right) + \varepsilon\left(\underline{x}\right) \tag{12}$$

where $\underline{x} = [x, y, \psi, u, v, r]^{\mathrm{T}}$ is the fuzzy system input, $\varepsilon\left(\underline{x}\right)$ is the minimum approximation error, satisfying $\left\| \varepsilon\left(\underline{x}\right) \right\| \leq \varepsilon^*$ with $\varepsilon^* > 0$, and $W$ is the ideal parameters vector.

$$W = \arg\min \left\{ \sup \left| f\left(\underline{x}\right) - \hat{W}^{\mathrm{T}} \xi\left(\underline{x}\right) \right| \right\} \tag{13}$$

The vessel dynamics (2) can be expressed as follows by introducing the fuzzy estimator (12) to handle the system uncertainties $f(\underline{x}) = -C(v)v - D(v)v - \Delta$:

$$M\dot{v} = W^{\mathrm{T}} \xi + \varepsilon + \tau + d + \sigma + \tau_m \tag{14}$$

To proceed with the control design, we integrated a novel filter to enhance the control performance of dynamic surface control. It increases the convergence rate to provide a fast response and better adaptation to rapidly changing arctic environments.

**Theorem 1.** *Regard a first-order filter with the following form (Wang, Wang, Wang, Zong and Hua, 2021):*

$$\dot{\bar{\phi}}_1 = \frac{\phi_1 - \bar{\phi}_1}{T_f} + \frac{\chi_1 \left(\phi_1 - \bar{\phi}_1\right)}{\left\| \phi_1 - \bar{\phi}_1 \right\|^{\frac{1}{2}} + \chi_2} \tag{15}$$

*If the input's derivative $\dot{\phi}_1$ is bounded, there exist positive constant matrices $T_f$, $\chi_1$, and $\chi_2$ which make the filter error $e_f = \bar{\phi}_1 - \phi_1$ arbitrarily small in a finite time.*

The proof of Theorem 1 is detailed in Appendix A.

**Remark 3.** Note that the proposed filter (15) can be reduced to a conventional first-order filter when $\chi_1 = 0$. It differs from the conventional filter in that it enables the filtered error signal to converge in finite time with a fast convergence rate. Additionally, the selection range of parameter $\chi_2$ is increased by the denominator's fractional order power.

The filter (15) is introduced to complete the dynamic surface control following two steps below.

Step 1: The first dynamic surface $s_1 \in R^3$ describing the position error is defined as

$$s_1 = \eta - \eta_d \tag{16}$$

A virtual control law $\alpha_1 \in R^3$ is designed to stabilize $s_1$.

$$\alpha_1 = J^{-1} \left( -k_1 s_1 + \dot{\eta}_d \right) \tag{17}$$

where $k_1 \in R^{3\times3}$ is a positive definite diagonal matrix.

Then, $\alpha_1$ is fed into the introduced filter. It is practical to replace $\dot{\alpha}_1$ with $\dot{\bar{\alpha}}_1$ to avoid multiple differentiation.

$$\dot{\bar{\alpha}}_1 = \frac{\alpha_1 - \bar{\alpha}_1}{T_f} + \frac{\chi_1 \left(\alpha_1 - \bar{\alpha}_1\right)}{\left\| \alpha_1 - \bar{\alpha}_1 \right\|^{\frac{1}{2}} + \chi_2} \tag{18}$$

The filter error is defined as

$$\tilde{\alpha} = \bar{\alpha}_1 - \alpha_1 \tag{19}$$

Step 2: The second dynamic surface $s_2 \in R^3$, describing the velocity error, is defined as

$$s_2 = v - \bar{\alpha}_1 \tag{20}$$

It follows from (14) that the derivative of $s_2$ is

$$\dot{s}_2 = M^{-1} \left( W^{\mathrm{T}} \xi + \varepsilon + \tau + d + \sigma + \tau_m \right) - \dot{\bar{\alpha}}_1 \tag{21}$$

Finally, we have a robust nonlinear control law for the position mooring system.

$$\tau = -k_2 s_2 + M\dot{\bar{\alpha}}_1 - \hat{W}^{\mathrm{T}} \xi - \hat{d} - \tau_m \tag{22}$$

where $k_2 \in R^{3\times3}$ is a positive definite diagonal matrix. $\hat{d}$ is the estimation of $d$ in (5) by the ice-load disturbance observer designed in the next subsection.

The adaptive law $\hat{W}$ is designed to update the parameters of fuzzy estimator (12) as follows

$$\dot{\hat{W}} = \Gamma \left( \xi\left(\underline{x}\right) s_2 - \gamma \hat{W} \right) \tag{23}$$

where $\Gamma$ is a positive definite adaptation gain matrix, $\gamma$ is a parameter matrix.

### 3.3. Ice-load disturbance observer design

According to Assumption 2 and Remark 2, an ice-load disturbance observer is constructed to address the discontinuous and non-smoothness ice-loads. It is independent of the prior assumption that the disturbance and its derivative are bounded.

An auxiliary vector of observer is described as

$$\varsigma = d - k_\varsigma M s_2 \tag{24}$$

where $k_\varsigma \in R^{3\times3}$ is a positive definite diagonal matrix.

In the light of (21), the derivative of $\varsigma$ is

$$\dot{\varsigma} = \dot{d} - k_\varsigma \left( W^{\mathrm{T}} \xi + \varepsilon + \tau + d + \sigma + \tau_m - M\dot{\bar{\alpha}}_1 \right) \tag{25}$$

Then the estimate of $\varsigma$ is designed as

$$\dot{\hat{\varsigma}} = -k_\varsigma \left( \hat{W}^{\mathrm{T}} \xi + \tau + \hat{\varsigma} + k_\varsigma M s_2 + \tau_m - M\dot{\bar{\alpha}}_1 \right) \tag{26}$$

From (24) and (26), we construct the ice-load disturbance observer.

$$\hat{d} = \hat{\varsigma} + k_{\varsigma} M s_2 \tag{27}$$

Let us define $\tilde{d} = d - \hat{d} = \varsigma - \hat{\varsigma} = \tilde{\varsigma}$ as the estimation error of the observer, we have $\dot{\tilde{d}}$ from (21), (26) and (27)

$$\begin{aligned} \dot{\tilde{d}} &= \dot{d} - \dot{\hat{d}} \\ &= \dot{d} - \left(\dot{\hat{\varsigma}} + k_{\varsigma} M \dot{s}_2\right) \\ &= \dot{d} - k_{\varsigma}\left(\tilde{W}^{\mathrm{T}}\xi + \tilde{\varsigma} + \varepsilon + \sigma\right) \end{aligned} \tag{28}$$

**Remark 4.** It is obvious from (28) that a differentiable disturbance is necessary for the ordinary disturbance observer. In contrast to that, the suggested observer (27) effectively handles discontinuous ice-loads owing to disturbance reconstruction (5). Additionally, it requires no prior assumption of the derivative boundedness and further resolves the unknown $D$ by the invariant set theory.

**Theorem 2.** *For the arctic moored vessel (1) and (2) with unknown time-varying environmental disturbances and unknown system uncertainties under Assumption 1 and 2, the proposed arctic position mooring robust control law (22) consists of a fuzzy estimator (12), a novel first-order filter (18), an adaptive law (23) and an ice-load disturbance observer (27). For all $V(0) < B_0$ with $B_0$ being any positive constant, all signals of the closed-loop system are guaranteed to be uniformly ultimately bounded. And the position error $s_1$, the adaptive gain error $\tilde{W}$ and the observer estimation error $\tilde{d}$ are settled respectively within the following compact sets:*

$$\Omega_{s_1} = \left\{ s_1 \in R^3 \,\middle|\, \|s_1\| \le \sqrt{\frac{\rho}{\mu}} \right\} \tag{29}$$

$$\Omega_{\tilde{W}} = \left\{ \tilde{W} \in R^{3\times N} \,\middle|\, \|\tilde{W}\| \le \sqrt{\frac{\rho/\mu}{\lambda_{\max}\left(\Gamma^{-1}\right)}} \right\} \tag{30}$$

$$\begin{aligned} \Omega_{\tilde{d}} = \Bigg\{ \tilde{d} \in R^3 \,\Big|\, \|\tilde{d}\| \le \frac{2D^*}{\lambda_{\max}\left(k_{\varsigma}\right)} + 2\left(\varepsilon^* + \sigma^*\right) \\ +2\sqrt{\frac{\rho/\mu}{\lambda_{\max}\left(\Gamma^{-1}\right)}} \Bigg\} \end{aligned} \tag{31}$$

Theorem 2 states that the proposed closed-loop control system is stable and that all of its signals are bounded. Appendix B provides a detailed description of the stability analysis.

A pseudo-code description of the proposed position mooring scheme implementation is provided in Table 1. In initialization phase, the simulation time, initial state of ship, desired reliability index, and control parameters are set. Note that the desired structural reliability is determined through simulations under extreme conditions based on the mooring system characteristics to prevent cable breakage. To generate the reference path, we use the improved setpoint chasing algorithm to minimize the objective function (7) while satisfying the constraints. Equation (8) is substituted into equation (6) to obtain the relationship between position increment, heading, and structural reliability. It follows from the relationship that the objective function with nonlinear constraints can be solved by the interior point method and the optimal solution, position increment and heading, is obtained. The smooth reference path (10) through the ideal setpoints can then be obtained. Subsequently, the fuzzy logic system (12) and the ice-load disturbance observer (27) are designed to handle system uncertainty and external disturbances, respectively. The adaptive dynamic surface control law (22) is designed to track the reference path and compensate for the disturbance estimation. In this way, an improved setpoint chasing algorithm provides the reference path that meets the requirements of cable safety and system energy consumption, and the observer-based adaptive fuzzy dynamic surface controller tracks the reference path, so that a safe and energy-efficient mooring positioning operation is achieved.

**Remark 5.** The proposed safe and energy-efficient arctic position mooring control scheme has the following application scope and limitations:

1. This paper investigates the regional position mooring of the ships. Due to the limitations of the mooring system, the position mooring system's operating water depth typically ranges from 300–400 m to 1500 m (American Petroleum Institute, 1996). The applied water depth in this paper should therefore fall within the aforementioned range.
2. The application scenario is in arctic, and the environmental disturbance contains wind, waves, currents, and sea ice, with ice load accounting for the main part. We only consider managed ice with discontinuous and non-smooth behavior and a fast change rate.
3. The proposed ice-load disturbance observer is for discontinuous disturbances without requiring bounded derivatives.
4. The interaction of mooring cables places restrictions on the improved setpoint chasing algorithm, making it unable to regulate the structural reliability indices of all cables to the desired value.

## 4. Numerical simulation results and discussion

Numerical simulations have been conducted on a turret-moored floating production storage and offloading (FPSO) vessel to evaluate the effectiveness and robustness of the proposed arctic position mooring control system. The comparative simulations with the state of the art demonstrate clearly the advantages of the proposed control scheme.

**Table 1**
The algorithm implementation.

| Algorithm: | Adaptive fuzzy dynamic surface control based setpoint chasing position mooring scheme |
|---|---|
| 1: | ***Initialization*** Set $t = 0$, $\eta(t)$, $\delta_d$ and control parameters; |
| 2: | ***Procedure*** |
| 3: | ***While*** The controller is not stopped ***do*** |
| 4: | Calculate the mooring tension $T_i$; |
| 5: | Solve the optimization objective function (7), find the optimal position increment $\Delta r$ and direction $\beta$; |
| 6: | Generate the smooth reference path $\eta_d$ (10); |
| 7: | Generate the estimation using the fuzzy logic system (12): $-C(\nu)\nu - D(\nu)\nu - \Delta = W^{\mathrm{T}}\xi\left(\underline{x}\right) + \varepsilon\left(\underline{x}\right)$; |
| 8: | Design the dynamic surfaces $s_1(t)$ (16) and $s_2(t)$ (20); |
| 9: | Design ice-load disturbance observer (27): $d \to \hat{d}$; |
| 10: | Generating control law (22) and adaptive update law (23): $s_1(t) \to 0$; |
| 11: | ***end while***; |
| 12: | $t = t + 1$; |
| 13: | ***end procedure***; |
| 14: | Complete the setpoint chasing position mooring task. |

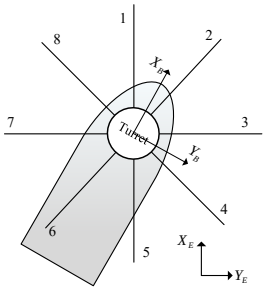


**Figure 4:** Mooring cable arrangement

## 4.1. Performance of the designed control law

In this scenario, the effectiveness of the proposed control strategy is illustrated in a time-varying arctic environmental disturbance considering ice loads.

The FPSO vessel considered in simulations has the following characteristics (Sangsoo and Kim, 2003): vessel length $L = 310m$, vessel width $B = 47.2m$, mass $m = 240869ton$ and yaw rotational inertia $I_z = 1.34 \times 10^{12} Kg \cdot m^2$. The dynamic parameter matrices $M$, $C(\nu)$, and $D(\nu)$ are calculated by using the corresponding parameters (Fossen, 2013). The system uncertainties term is set to $\Delta = 0.1\sin(0.001t)M + 0.1\cos(0.001t)C(\upsilon) + 0.1\sin(0.001t)D(\upsilon)$. The considered mooring system includes eight cables attached to the turret (Wang et al., 2018), as illustrated in Fig.4, symmetrically anchored at $(800, 0)$, $(0, 800)$, $(-800, 0)$, $(0, -800)$, $(565.69, 565.69)$, $(-565.69, 565.69)$, $(-565.69, -565.69)$ and $(565.69, -565.69)$ following the order of cables No. 1 to No. 8.

The time-varying environmental disturbances consist of wind, waves, currents, and ice. The ice loads are imitated with a controllable pack ice model as shown in Fig.2 (Lee et al., 2019), and the other disturbances are described by relevant empirical formulas (Fossen, Thor I., 2011). We set the sea state as wind velocity $u_w = 8m/s$, wind direction $\alpha_w = 45°$, current velocity $u_c = 0.4m/s$, current direction $\alpha_c = 60°$, significant wave height $h_s = 2m$, wave direction $\alpha_{wave} = 15°$ and wave period $T = 8.61s$.

The control objective is to maintain the vessel within a safe region in an energy-efficient manner. The region radius $r_{\max} = 110.91m$ is determined by simulations under extreme environment. The desired heading is $10°$, the critical and the desired structural reliability are set to $\delta_c = 3$ and $\delta_d = 4$ while respecting the constraint $\delta_d \geq \delta_c$. The reference position of the vessel is generated by the proposed setpoint chasing algorithm. The initial states of FPSO vessel in terms of position and velocity are $\eta(0) = [0, 0, 0]^{\mathrm{T}}$ and $\nu(0) = [0, 0, 0]^{\mathrm{T}}$.

The control design parameters are chosen as: $a_i = 1$, $k_1 = diag(2, 2, 2), T_f = diag(1, 1, 1), \chi_1 = diag(10, 10, 10)$, $\chi_2 = [1, 1, 1]^{\mathrm{T}}$, $k_2 = diag(3, 3, 3)$, $\Gamma_1 = \Gamma_2 = 10^3 I_{3^6 \times 3^6}$, $\Gamma_3 = 10^5 I_{3^6 \times 3^6}$, $\gamma_1 = \gamma_2 = 10^{-3}$, $\gamma_3 = 10^{-5}$ and $k_\varsigma = diag(5, 5, 5)$.

**Remark 6.** Parameters selection criteria: (i) The mooring system does not involve special cases, equally treats all cables with $a_i = 1$. And the weighting factor can be adjusted according to the cable importance while considering specific applications such as fault-tolerant control and cable breakage. (ii) As for the filter parameters, $\chi_1$ and $\chi_2$ are chosen large enough and small enough to satisfy Theorem 1, respectively, so that the filter error converges to arbitrarily small and the inequality condition of the filter design is easily achieved. (iii) The control parameters should follow Theorem 2, increasing $k_1$, $k_2$, $\gamma$, $k_\varsigma$, and decreasing $\gamma$. In this way, it is obvious that (B.11) and $\mu > \frac{\rho}{2B_0} > 0$ hold. Accordingly, all system signals are uniformly ultimately

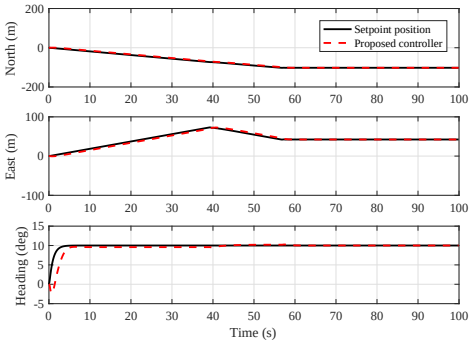


**Figure 5:** North, east position and heading of the FPSO vessel.

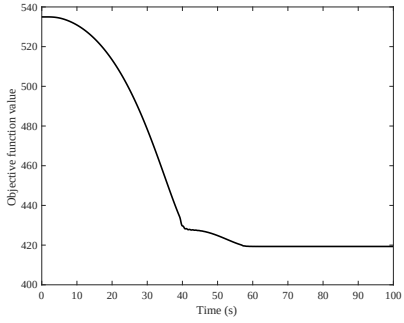


**Figure 6:** Evolution of the objective function of the proposed control strategy.

bounded and converge to an arbitrarily small neighborhood of zero.

The obtained simulation results are depicted in Figs.5-10.

Fig.5 illustrates the position and heading of the FPSO vessel as it follows the reference setpoint. It shows that the vessel is precisely positioned at the reference setpoint, and the dynamic surface control law provides a satisfactory control performance for quickly following the setpoint with small errors under time-varying disturbances. According to the objective function in Fig.6, it is clear that its value rapidly falls and then maintains the minimum, indicating that the proposed setpoint chasing algorithm effectively exploits the mooring system's capacity. The simulation results of the mooring system depicting the structural reliability index and tension are shown in Fig.7. Cables 1 and 8 achieve the desired structural reliability index in Fig.7(a), and provide more mooring forces in Fig.7(b). It illustrates that the proposed control strategy considers all the mooring system cables in addition to the critical one. However, the cable arrangement in Fig.4 causes some mooring tension to increase while others decreases as the ship position changes. Similar variations can be found in the structural reliability. It follows that the sepoint chasing algorithm can only regulate part of the cable structural reliability to the desired value, while satisfying the constrained objective function (7). Consequently, combined with the position in Fig.5, only cables 1 and 8

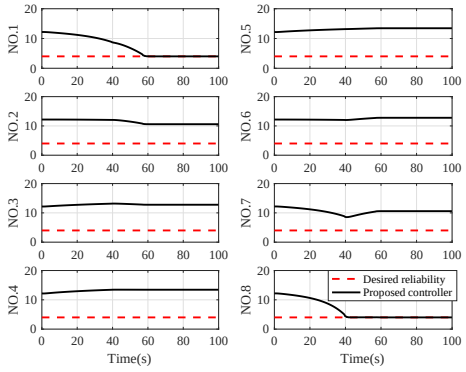


(a) Structural reliability index of mooring cables.

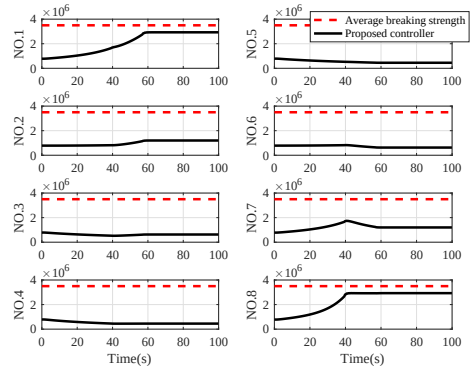


(b) Mooring cable tensions.

**Figure 7:** Simulation results of the mooring system.

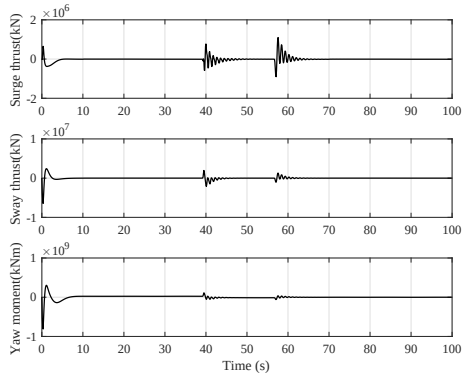


**Figure 8:** Evolution versus time of the forces and moment of the proposed controller.

reach the desired structural reliability. Moreover, the safety of the FPSO vessel is ensured since the structural reliability indices are larger than the critical value and the mooring forces are smaller than the mean breaking strength.

Fig.8 illustrates the evolution versus time of the control forces of the proposed controller, maneuvering the positron and heading of the FPSO vessel following the generated setpoint and resisting the environmental disturbances beyond the capacity of the mooring system. It is worth noting

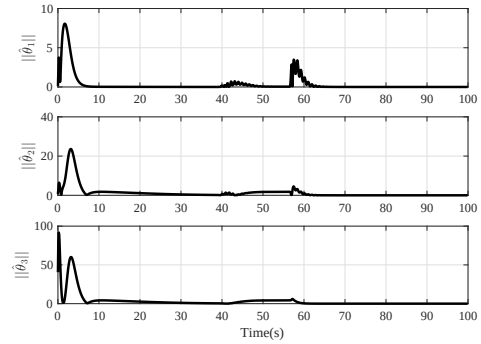


**Figure 9:** The parameter estimate vectors of the fuzzy logic system.

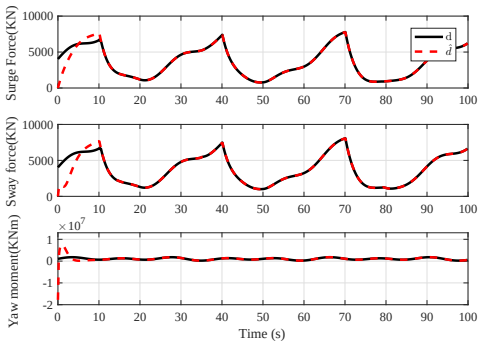


**Figure 10:** Estimation of the proposed disturbance observer.

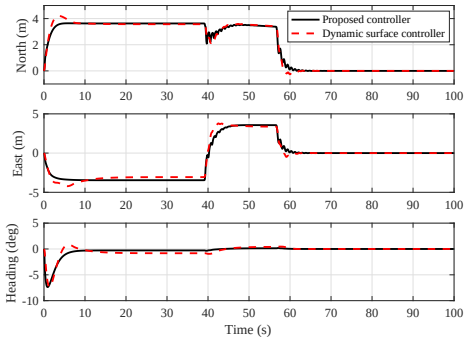


**Figure 11:** Evolution versus time of the setpoint chasing error of both controllers.

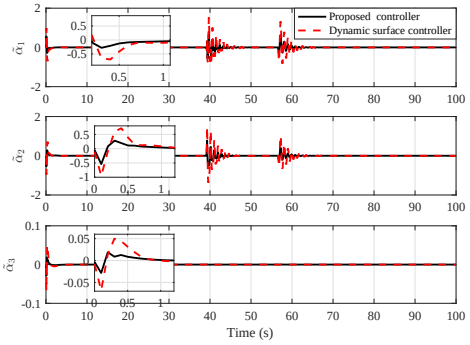


**Figure 12:** Evolution versus time of the filter error of the dynamic surface controller.

from Fig.7 that most of the disturbance is compensated by mooring cables No.1 and 8 simultaneously. As the tension increases with the number of cables carrying the environmental loads, the required control effort decreases. Fig.9 and Fig.10 demonstrate that the proposed fuzzy estimator and disturbance observer are able to estimate the system uncertainties and environmental disturbances. Additionally, Theorem 2's conclusion regarding the boundedness of the adaptive gain and observer parameters is also demonstrated.

To sum up, it can be concluded that the proposed arctic position mooring control scheme achieves the control objective and provides effective, robust, safe and energy efficient control performance in the presence of system uncertainties and environmental disturbances with discontinuous ice loads.

## 4.2. Comparison with other control schemes

The conducted comparative simulations include three case studies: (i) The first simulation compares the suggested control with the typical dynamic surface control to show the benefits of the proposed control law; (ii) The second comparison is conducted with the reliability-based control to demonstrate the energy efficiency of the suggested setpoint chasing based position mooring control scheme; (iii) The last part is dedicated to illustrating the effectiveness and safety of the improved setpoint chasing algorithm.

**Case Study 1:** The dynamic surface control law (Du, Hu, Krstic and Sun, 2016) for the comparison is expressed as follows .

$$\tau_{DSC} = -k_2 s_2 + M\dot{\bar{\alpha}}_2 - \hat{W}^{\mathrm{T}}\xi - \hat{d} - \tau_m \tag{32}$$

where $T_d\dot{\bar{\alpha}}_{11}+\bar{\alpha}_{11} = \alpha_1$ is the first-order filter of the dynamic surface comparative controller. The control parameters are set the same as our proposed controller.

The setpoint chasing error and the filter error are depicted in Figs.11 and 12, respectively. It is evident from Fig.11 that the reference setting path can be successfully followed by both controllers. However, the proposed controller provides better control performance with a smaller tracking error and a higher convergence rate. Fig. 12 illustrates that the novel filter apparently provides faster convergence speed and smaller overshoot than the state-of-the-art filter. Consequently, the proposed improved dynamic surface control law outperforms the existing one.

**Case Study 2:** A structural reliability-based control strategy that directly introduces structural reliability as a controlled variable (Wang et al., 2018) is implemented for this comparison.

$$\begin{aligned}\tau_\delta = MQ^{-1}\left(-k_{\delta 2}s_{\delta 2} + \dot{\bar{\alpha}}_{\delta 1} - \dot{Q}\upsilon\right) + C(\upsilon)\upsilon \\ + D(\upsilon)\upsilon - \tau_m - \tau_{env}\end{aligned} \tag{33}$$

The design parameters of this controller are set the same as the proposed controller.

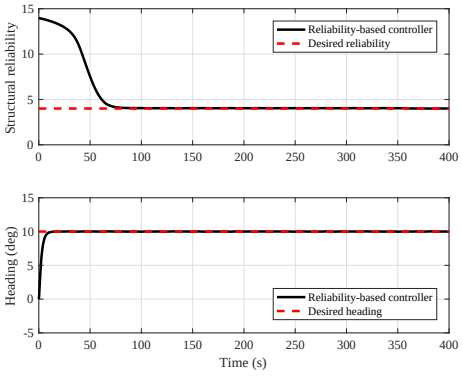


**Figure 13:** Evolution versus time of the control performance of the structural reliability-based controller.

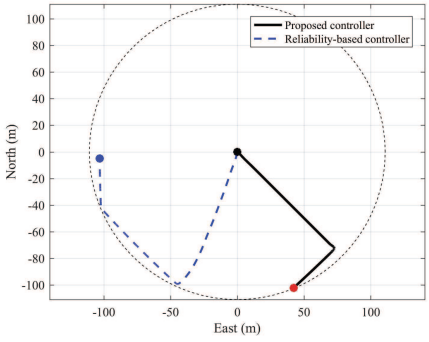


**Figure 14:** Trajectory of the FPSO vessel for both control strategies.

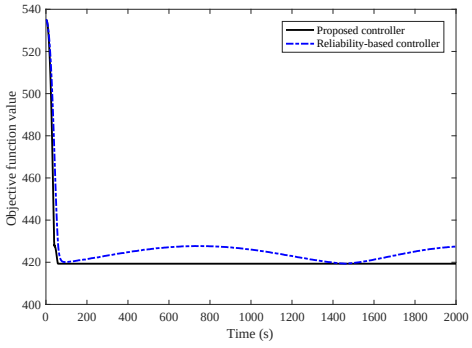


**Figure 15:** Evolution versus time of the cost function for both control strategies.

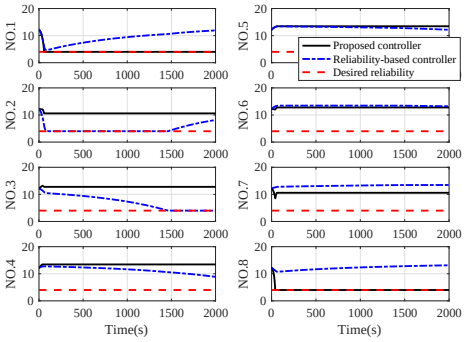


**Figure 16:** Evolution versus time of the structural reliability indices of the mooring cables.

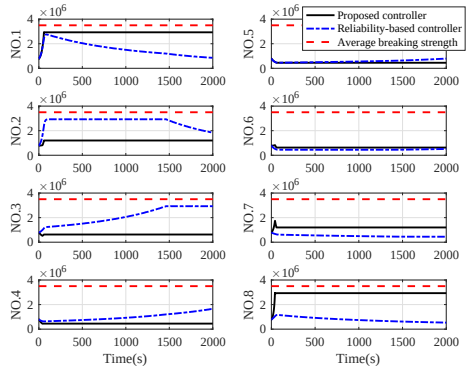


**Figure 17:** Evolution versus time of the mooring tensions of the cables.

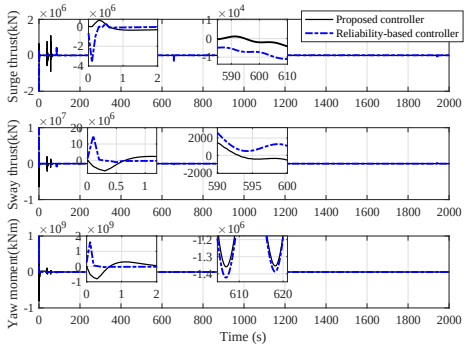


**Figure 18:** Evolution versus time of the forces and moment of both control strategies.

The obtained simulation results are depicted in Figs.13-18. It can be clearly seen from Fig.13 that the reliability-based controller enables the critical reliability and heading to reach and maintain their desired values. Although both controllers keep the vessel's trajectory in Fig.14 within the safe region, the proposed controller's trajectory is shorter and simpler than the state-of-the-art controller's. From the objective function evolution in Fig.15, the proposed controller provides more stable performance. In that the comparative structural reliability-based controller introduces the structural reliability index rather than position variation, stabilizing the error between the desired value and the minimum reliability index at zero, only the one critical cable with the lowest structural reliability index can be regulated. So that the critical cable of comparative controller in Fig.16 shifts over time from No. 1 to No. 2 and then to No. 3. It suggests that the objective function of the comparative controller fluctuates and cannot be kept at a constant minimum. It thus obviously illustrates that the setpoint-based

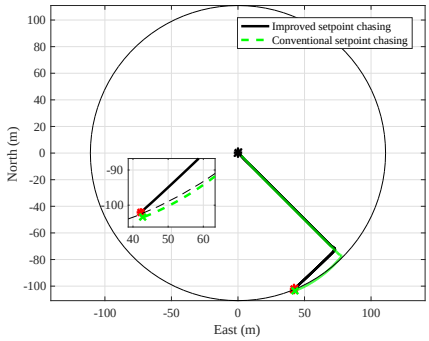


**Figure 19:** The trajectories of the FPSO vessel under the two setpoint chasing algorithms.

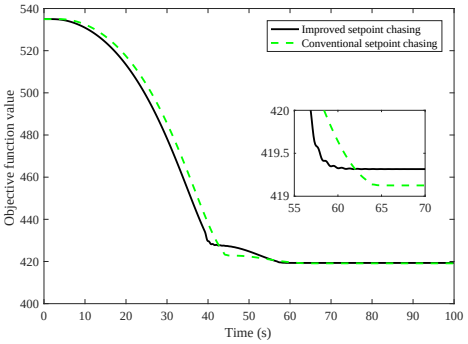


**Figure 21:** Evolution of the cost function for the two setpoint chasing algorithms.

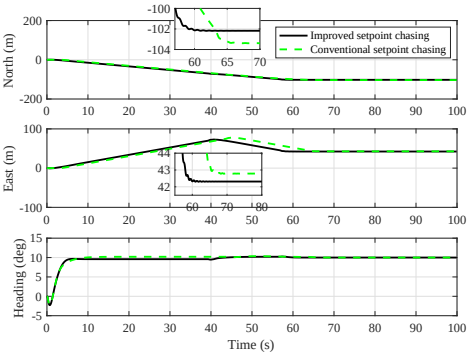


**Figure 20:** North and east positions and headings of the FPSO vessel using the two setpoint chasing algorithms.

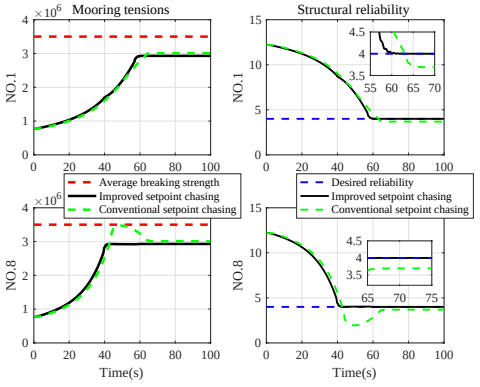


**Figure 22:** Simulation results of the mooring system.

control scheme provides a more effective strategy, as it simultaneously considers all mooring cables.

Fig.17 shows the evolution of the mooring forces, the reliability-based controller regulates only one cable at a time, whereas the proposed controller can regulates multiple cables. Thus, the capacity of the mooring system is used to its full potential, resulting in a reduction in the required thruster force. It can be verified from Fig.18 that the reliability-based controller requires more control forces than the proposed controller. As a result, the proposed setpoint chasing controller achieves a more energy efficient position mooring control.

**Case Study 3:** The conventional setpoint chasing algorithm (Fang et al., 2013) without structural reliability constraints is considered for this simulation scenario. The obtained results are shown in Figs.19-22. Only the relevant notable cable is depicted, since the others are far from the critical value.

From Fig.19, it is obvious that the vessel trajectory is constrained within the safe region by the improved algorithm. Contrarily, the conventional algorithm regulates the trajectory exceed the safe margin, and has its final setpoint outside the safe region as seen in Fig.20. In addition, although the improved algorithm's objective function value in Fig.21 is higher than that of the conventional algorithm, the lack of reliability constraint in the conventional algorithm leads to tension exceeding the average breaking strength and structural reliability below the available minimal value in Fig.22. This can result in cable breakage and compromises the security of the operation. Therefore, in order to guarantee the safety of the mooring system, the structural reliability constraints are crucial for the setpoint chasing algorithm.

In conclusion, the improved setpoint chasing algorithm introduces the structural reliability constraints, ensuring that reliability stays above its critical value, maintaining the probability of cable breakage within tolerance and consequently enhancing the safety of the mooring system.

## 5. Conclusion and future works

This paper investigated an arctic position mooring control scheme in the presence of system uncertainties and ice load disturbances. The safety and energy-efficiency coordination issues of the position mooring system are handled by the improved setpoint chasing algorithm introducing structural reliability constraints. The restrictive assumption that the disturbance is smooth, continuous, and derivatively bounded is removed by the ice-load disturbance observer. The proposed adaptive fuzzy dynamic surface control law improves the convergence speed and enhances the control

performance. Theoretical analysis verified the system stability and the uniform ultimate boundedness of all the closed-loop system signals. Comparative simulation studies clearly demonstrate that our proposed control scheme provides an effective, robust, safe, and energy efficient position mooring control. The proposed position mooring control scheme can be safely applied to arctic marine resource exploration. As for future work, input saturation of thrusters can be considered to further improve the safety and practicality.

# Appendix

## A. Proof on Theorem 1

PROOF. Let us define the following Lyapunov function

$$V_f = \frac{1}{2} e_f^{\mathrm{T}} e_f \tag{A.1}$$

It follows from (A.1) that the time derivative of $V_f$ yields

$$\begin{aligned}
\dot{V}_f &= e_f^{\mathrm{T}} \left( -\frac{e_f}{T_f} - \frac{\chi_1 e_f}{\left( \left\| e_f \right\|^{\frac{1}{2}} + \chi_2 \right)} - \dot{\phi}_1 \right) \\
&\leq -\frac{e_f^{\mathrm{T}} e_f}{T_f} - \frac{\chi_1 \left\| e_f \right\|^2}{\left\| e_f \right\|^{\frac{1}{2}} + \chi_2} + \left\| e_f \right\| \left\| \dot{\phi}_1 \right\| \\
&\leq -\left\| e_f \right\|^{\frac{1}{2}} \left( \frac{\chi_1 \left\| e_f \right\|^{\frac{3}{2}}}{\left\| e_f \right\|^{\frac{1}{2}} + \chi_2} - \left\| e_f \right\|^{\frac{1}{2}} \left\| \dot{\phi}_1 \right\| \right) \\
&\quad - \frac{e_f^{\mathrm{T}} e_f}{T_f}
\end{aligned} \tag{A.2}$$

If the bounded input $\left\| \dot{\phi}_1 \right\| \leq \phi_m$, there exists $\kappa > 1$ such that $\chi_1 = \kappa \phi_m > \left\| \dot{\phi}_1 \right\|$, then (A.2) leads to

$$\begin{aligned}
\dot{V}_f &\leq -\left\| e_f \right\|^{\frac{1}{2}} \left( \frac{\kappa \phi_m \left\| e_f \right\|^{\frac{3}{2}}}{\left\| e_f \right\|^{\frac{1}{2}} + \chi_2} - \left\| e_f \right\|^{\frac{1}{2}} \phi_m \right) - \frac{e_f^{\mathrm{T}} e_f}{T_f} \\
&\leq -\left\| e_f \right\|^{\frac{1}{2}} \phi_m \left( \frac{\kappa \left\| e_f \right\|^{\frac{3}{2}}}{\left\| e_f \right\|^{\frac{1}{2}} + \chi_2} - \left\| e_f \right\|^{\frac{1}{2}} \right) - \frac{e_f^{\mathrm{T}} e_f}{T_f}
\end{aligned} \tag{A.3}$$

If inequality $\left\| e_f \right\| \geq \sqrt{\frac{(\chi_2+1)^2}{4(\kappa-1)^2} + \frac{\chi_2}{\kappa-1}}$ holds, then

$$\begin{aligned}
\dot{V}_f &\leq -\frac{e_f^T e_f}{T_f} - \left\| e_f \right\|^{\frac{3}{2}} \phi_m \\
&= -\frac{2}{T_f} V_f - 2^{\frac{3}{4}} \phi_m V_f^{\frac{3}{4}}
\end{aligned} \tag{A.4}$$

Consequently, the filter error can converge to the set $\Omega_{e_f} = \left\{ e_f \left| \left\| e_f \right\| \leq \sqrt{\frac{(\chi_2+1)^2}{4(\kappa-1)^2} + \frac{\chi_2}{\kappa-1}} \right. \right\}$ in a finite time, which can be made arbitrary small by appropriately adjusting the parameters $\kappa$ large and $\chi_2$ small. In this way, $\| e_f \|$ can easily fulfill the inequality condition.

## B. Stability analysis of the arctic position mooring system

Choose the following Lyapunov function for the whole system.

$$V = \frac{1}{2} s_1^{\mathrm{T}} s_1 + \frac{1}{2} s_2^{\mathrm{T}} M s_2 + \frac{1}{2} \tilde{W}^{\mathrm{T}} \Gamma^{-1} \tilde{W} + \frac{1}{2} \tilde{\alpha}^{\mathrm{T}} \tilde{\alpha} + \frac{1}{2} \tilde{d}^{\mathrm{T}} \tilde{d} \tag{B.5}$$

The time derivative of $V$ leads to the following result.

$$\dot{V} = s_1^{\mathrm{T}} \dot{s}_1 + s_2^{\mathrm{T}} M \dot{s}_2 + \tilde{W}^{\mathrm{T}} \Gamma^{-1} \dot{\tilde{W}} + \tilde{\alpha}^{\mathrm{T}} \dot{\tilde{\alpha}} + \tilde{d}^{\mathrm{T}} \dot{\tilde{d}} \tag{B.6}$$

It follows from (16), (17), (19), (20), $\| J(\eta) \| = 1$ and Young's inequality that

$$\begin{aligned}
s_1^{\mathrm{T}} \dot{s}_1 &= s_1^{\mathrm{T}} \left( J \left( s_2 + \bar{\alpha}_1 \right) - \dot{\eta}_d \right) \\
&= s_1^{\mathrm{T}} \left( J s_2 + J \left( \tilde{\alpha} + J^{-1} \left( -k_1 s_1 + \dot{\eta}_d \right) \right) - \dot{\eta}_d \right) \\
&= s_1^{\mathrm{T}} \left( J s_2 + J \tilde{\alpha} - k_1 s_1 \right) \\
&\leq -s_1^{\mathrm{T}} k_1 s_1 + s_1^{\mathrm{T}} s_1 + \frac{1}{2} s_2^{\mathrm{T}} s_2 + \frac{1}{2} \tilde{\alpha}^{\mathrm{T}} \tilde{\alpha}
\end{aligned} \tag{B.7}$$

In the light of (21) and (22), we have

$$\begin{aligned}
s_2^{\mathrm{T}} M \dot{s}_2 &= s_2^{\mathrm{T}} \left( W^{\mathrm{T}} \xi + \varepsilon + \tau + d + \sigma + \tau_m - M \dot{\bar{\alpha}}_1 \right) \\
&= -s_2^{\mathrm{T}} k_2 s_2 + s_2^{\mathrm{T}} \tilde{W}^{\mathrm{T}} \xi + s_2^{\mathrm{T}} \left( \tilde{d} + \sigma + \varepsilon \right)
\end{aligned} \tag{B.8}$$

According to (12), (23) and Young's inequality, we deduce

$$\begin{aligned}
\tilde{W}^{\mathrm{T}} \Gamma^{-1} \dot{\tilde{W}} &= \tilde{W}^{\mathrm{T}} \Gamma^{-1} \left( \dot{W} - \dot{\hat{W}} \right) \\
&= -\tilde{W}^{\mathrm{T}} \xi s_2 + \gamma \tilde{W}^{\mathrm{T}} \hat{W} \\
&\leq -\tilde{W}^{\mathrm{T}} \xi s_2 - \frac{\gamma}{2} \tilde{W}^{\mathrm{T}} \tilde{W} + \frac{1}{2} W^{\mathrm{T}} W
\end{aligned} \tag{B.9}$$

Using $\tilde{d} = \tilde{\varsigma}$ and (28) yield

$$\begin{aligned}
\tilde{d}^{\mathrm{T}} \dot{\tilde{d}} &= \tilde{d}^{\mathrm{T}} \dot{d} - \tilde{d}^{\mathrm{T}} k_\varsigma \left( \tilde{W}^{\mathrm{T}} \xi + \varepsilon + \sigma \right) - \tilde{d}^{\mathrm{T}} k_\varsigma \tilde{d} \\
&= -\frac{1}{2} \tilde{d}^{\mathrm{T}} k_\varsigma \tilde{d} - \left[ \frac{1}{2} \tilde{d}^{\mathrm{T}} k_\varsigma \tilde{d} - \tilde{d}^{\mathrm{T}} \dot{d} \right. \\
&\quad \left. + \tilde{d}^{\mathrm{T}} k_\varsigma \left( \tilde{W}^{\mathrm{T}} \xi + \varepsilon + \sigma \right) \right]
\end{aligned} \tag{B.10}$$

Then, we obtain $\tilde{d}^{\mathrm{T}} \dot{\tilde{d}} \leq -\frac{k_\varsigma}{2} \tilde{d}^{\mathrm{T}} \tilde{d} < 0$, as long as

$$\left\| \tilde{d} \right\| \geq \frac{2D}{k_\varsigma} + 2 \left\| \tilde{W} \right\| + 2 \left( \varepsilon^* + \sigma^* \right) \tag{B.11}$$

Recalling (A.4) and substituting (B.7) - (B.11) into (B.6), leads to

$$\begin{aligned}
\dot{V} &\leq -s_1^{\mathrm{T}} k_1 s_1 + s_1^{\mathrm{T}} s_1 + \frac{1}{2} s_2^{\mathrm{T}} s_2 + \frac{1}{2} \tilde{\alpha}^{\mathrm{T}} \tilde{\alpha} - s_2^{\mathrm{T}} k_2 s_2 \\
&\quad + s_2^{\mathrm{T}} \left( \tilde{d} + \sigma + \varepsilon \right) - \frac{\gamma}{2} \tilde{W}^{\mathrm{T}} \tilde{W} + \frac{1}{2} W^{\mathrm{T}} W \\
&\quad - \frac{1}{T_f} \tilde{\alpha}^{\mathrm{T}} \tilde{\alpha} - \| \tilde{\alpha} \|^{\frac{3}{2}} \alpha_m - \frac{1}{2} \tilde{d}^{\mathrm{T}} k_\varsigma \tilde{d}
\end{aligned} \tag{B.12}$$

For harsh marine environments, especially for ice-loads with infinite energy, it should be noted that $\|\dot{d}\| < D$ with bounded $D$ cannot be known a priori. Hence, the upper bound of the disturbance derivative here is unknown. A compact set $\Omega$ is constructed to address this issue (Slotine, Li et al., 1991).

$$\Omega = \left\{ \left( s_1, s_2, \tilde{W}, \tilde{\alpha}, \tilde{d} \right) : V \leq B_0, \forall B_0 > 0 \right\} \quad \text{(B.13)}$$

Consequently, there exists a maximum $D^*$ of the continuous function $D$ on $\Omega$, such that $\left\|\tilde{d}\right\| \leq \frac{2D}{k_\varsigma} + 2\left\|\tilde{W}\right\| + 2\left(\varepsilon^* + \sigma^*\right)$ always holds. In view of $2s_2^{\mathrm{T}}\left\|\tilde{W}\right\| \leq \frac{4s_2^{\mathrm{T}}s_2}{\gamma} + \frac{\gamma\|\tilde{W}\|^2}{4}$, the derivative $\dot{V}$ is derived by Young's inequality.

$$\begin{aligned}
\dot{V} \leq & -s_1^{\mathrm{T}}k_1 s_1 + s_1^{\mathrm{T}}s_1 + \frac{1}{2}s_2^{\mathrm{T}}s_2 - s_2^{\mathrm{T}}k_2 s_2 \\
& - \frac{\gamma}{2}\tilde{W}^{\mathrm{T}}\tilde{W} + \frac{1}{2}W^{\mathrm{T}}W \\
& + \frac{1}{2}\tilde{\alpha}^{\mathrm{T}}\tilde{\alpha} - \frac{1}{T_f}\tilde{\alpha}^{\mathrm{T}}\tilde{\alpha} - \frac{1}{2}\tilde{d}^{\mathrm{T}}k_\varsigma\tilde{d} \\
& + s_2^{\mathrm{T}}\left(\frac{2D^*}{k_\varsigma} + 2\left\|\tilde{W}\right\| + 3\left(\varepsilon^* + \sigma^*\right)\right) \\
\leq & -s_1^{\mathrm{T}}k_1 s_1 + s_1^{\mathrm{T}}s_1 - s_2^{\mathrm{T}}k_2 s_2 + s_2^{\mathrm{T}}s_2 + \frac{4}{\gamma}s_2^{\mathrm{T}}s_2 \\
& - \frac{\gamma}{4}\left\|\tilde{W}\right\|^2 + \frac{1}{2}\left\|2D^*/k_\varsigma + 3\left(\varepsilon^* + \sigma^*\right)\right\|^2 \\
& + \frac{1}{2}W^{\mathrm{T}}W + \frac{1}{2}\tilde{\alpha}^{\mathrm{T}}\tilde{\alpha} - \frac{1}{T_f}\tilde{\alpha}^{\mathrm{T}}\tilde{\alpha} - \frac{1}{2}\tilde{d}^{\mathrm{T}}k_\varsigma\tilde{d}
\end{aligned} \quad \text{(B.14)}$$

Furthermore, we have

$$\begin{aligned}
\dot{V} \leq & -\left[\lambda_{\min}\left(k_1\right) - 1\right]s_1^{\mathrm{T}}s_1 \\
& - \left[\lambda_{\min}\left(k_2\right) - 1 - \frac{4}{\gamma}\right]s_2^{\mathrm{T}}s_2 \\
& - \left[\lambda_{\min}\left(\frac{1}{T_f}\right) - \frac{1}{2}\right]\tilde{\alpha}^{\mathrm{T}}\tilde{\alpha} - \lambda_{\min}\left(\frac{k_\varsigma}{2}\right)\tilde{d}^{\mathrm{T}}\tilde{d} \\
& - \frac{\gamma}{4}\tilde{W}^{\mathrm{T}}\tilde{W} + \frac{1}{2}W^{\mathrm{T}}W \\
& + \frac{1}{2}\left\|\frac{2D^*}{k_\varsigma} + 3\left(\varepsilon^* + \sigma^*\right)\right\|^2 \\
\leq & -2\mu V + \rho
\end{aligned} \quad \text{(B.15)}$$

where $\rho = \frac{1}{2}\left\|\frac{2D^*}{k_\varsigma} + 3\left(\varepsilon^* + \sigma^*\right)\right\|^2 + \frac{1}{2}W^{\mathrm{T}}W$, positive design parameter $\mu = \min\left\{\lambda_{\min}\left(k_1\right) - 1, \frac{\lambda_{\min}(k_2) - 1 - 4/\gamma}{\lambda_{\max}(M)}, \lambda_{\min}(\frac{1}{T_f}) - \frac{1}{2}, \lambda_{\min}(\frac{k_\varsigma}{2})\right\}$, satisfying $\mu > \frac{\rho}{2B_0}$. $\lambda_{\min}$ and $\lambda_{\max}$ are the minimum and maximum eigenvalues of a matrix.

**Remark 7.** It is clear from (B.15) that there exists a compact set $\Omega$ such that $\dot{V} \leq -2\mu V + \rho$ holds. Appropriately adjust the parameters with increasing $k1$, $k2$, $\Gamma$ and $k_\varsigma$ to make $\frac{2\mu}{\rho}$ arbitrarily small, so that $\dot{V} < 0$ holds on $V = B_0$. Accordingly, $\Omega = \left\{\left(s_1, s_2, \tilde{W}, \tilde{\alpha}, \tilde{d}\right) : V \leq B_0, \forall B_0 > 0\right\}$ is an invariant set. This is to say, all the closed-loop system signals are always on $\Omega$ according to invariant set theory. Additionally, it is confirmed that the upper bound of disturbance derivative exists on $\Omega$ all the time.

From (B.15), it can be deduced that

$$0 \leq V(t) \leq \frac{\rho}{2\mu} + \left[V(0) - \frac{\rho}{2\mu}\right]\mathrm{e}^{-2\mu t} \quad \text{(B.16)}$$

Now, it is clear from (B.5) that $V(t)$ and $s_1$, $s_2$, $\tilde{W}$, $\tilde{\alpha}$ and $\tilde{d}$ are uniformly ultimately bounded. Then, it follows from (16), (19), (20), (23), and (28) that $\eta$, $\alpha_1$, $\bar{\alpha}_1$, $\nu$, $\hat{W}$ and $\hat{d}$ are uniformly ultimately bounded. Hence, all the signals of the resulting closed-loop system are proved to be uniformly ultimately bounded.

According to (B.16), we deduce that $V(t) \leq V(0) + \frac{\rho}{2\mu}$, and $\lim_{t\to\infty} V(t) = \frac{\rho}{2\mu}$. In view of $\frac{1}{2}s_1^T s_1 \leq V(t)$ and $\frac{1}{2}\tilde{W}^{\mathrm{T}}\Gamma^{-1}\tilde{W} \leq V(t)$, we denote $2\left[V(0) - \frac{\rho}{2\mu}\right]\mathrm{e}^{-2\mu t}$ by $V_m$ and obtain

$$\left\|s_1\right\| \leq \sqrt{\frac{\rho}{\mu} + V_m} \leq \sqrt{\frac{\rho}{\mu}} \quad \text{(B.17)}$$

$$\left\|\tilde{W}\right\| \leq \sqrt{\frac{\rho/\mu + V_m}{\lambda_{\max}\left(\Gamma^{-1}\right)}} \leq \sqrt{\frac{\rho/\mu}{\lambda_{\max}\left(\Gamma^{-1}\right)}} \quad \text{(B.18)}$$

Recalling (B.10), (B.11) and (B.18), yields

$$\left\|\tilde{d}\right\| \leq \frac{2D^*}{\lambda_{\min}\left(k_\varsigma\right)} + 2\left(\varepsilon^* + \sigma^*\right) + 2\sqrt{\frac{\rho/\mu}{\lambda_{\max}\left(\Gamma^{-1}\right)}} \quad \text{(B.19)}$$

Consequently, the proof of Theorem 2 is concluded.

## References


American Petroleum Institute, 1996. Recommended practice for design and analysis of stationkeeping systems for floating structures. American Petroleum Institute.

Bjørnø, J., Heyn, H.M., Skjetne, R., Dahl, A.R., Frederich, P., 2017. Modeling, parameter identification and thruster-assisted position mooring of c/s inocean cat i drillship, in: International Conference on Offshore Mechanics and Arctic Engineering, American Society of Mechanical Engineers. p. V07BT06A019.

Daley, C., Alawneh, S., Peters, D., Quinton, B., Colbourne, B., 2012. Gpu modeling of ship operations in pack ice, in: SNAME International Conference and Exhibition on Performance of Ships and Structures in Ice, pp. 122–127. doi:10.5957/ICETECH-2012-109. d021S005R001.

Du, J., Hu, X., Krstic, M., Sun, Y., 2016. Robust dynamic positioning of ships with disturbances under input saturation. Automatica 73, 207–214. doi:10.1016/j.automatica.2016.06.020.

Faltinsen, O., 1990. Sea loads on ships and offshore structures. New York, NY (United States); Cambridge University Press, United States.

Fang, S., Blanke, M., Leira, B.J., 2010. Optimal set-point chasing of position moored vessel, in: ASME 2010 29th International Conference on Ocean, Offshore and Arctic Engineering, pp. 479–486. doi:10.1115/omae2010-20812.

Fang, S., Blanke, M., Leira, B.J., 2015. Mooring system diagnosis and structural reliability control for position moored vessels. Control Engineering Practice 36, 12–26.

Fang, S., Leira, B.J., Blanke, M., 2013. Position mooring control based on a structural reliability criterion. Structual safety 41, 97–106.

Fossen, T.I., 1994. Guidance and Control of Ocean Vehicles. Wiley, Chichester;New York.

Fossen, T.I., 2013. Mathematical models of ships and underwater vehicles, in: Baillieul, J., Samad, T. (Eds.), Encyclopedia of Systems and Control. Springer London, London, pp. 1–9.

Fossen, T.I., Strand, J.P., 1999. Passive nonlinear observer design for ships using lyapunov methods: full-scale experiments with a supply vessel. Automatica 35, 3–16. doi:https://doi.org/10.1016/S0005-1098(98)00121-6.

Fossen, Thor I., 2002. Marine control systems: guidance, navigation and control of ships, rigs and underwater vehicles. volume 28. Springer.

Fossen, Thor I., 2011. Environmental forces and moments, in: Handbook of Marine Craft Hydrodynamics and Motion Control. John Wiley & Sons. chapter 8, pp. 187–225.

Gautier, D.L., Bird, K.J., Charpentier, R.R., Grantz, A., Houseknecht, D.W., Klett, T.R., Moore, T.E., Pitman, J.K., Schenk, C.J., Schuenemeyer, J.H., et al., 2009. Assessment of undiscovered oil and gas in the arctic. Science 324, 1175–1179.

He, H., Wang, L., Wang, X., Li, B., Xu, S., 2021. Energy-efficient control of a thruster-assisted position mooring system using neural q-learning techniques. Ships and Offshore Structures 16, 735–746.

Jayasiri, A., Nandan, A., Imtiaz, S., Spencer, D., Ahmed, S., 2016. An optimum control-based approach for dynamic positioning of vessels, in: Decision & Control, pp. 2796–2801.

Jayasiri, A., Nandan, A., Imtiaz, S., Spencer, D., Islam, S., Ahmed, S., 2017. Dynamic positioning of vessels using a ukf-based observer and an nmpc-based controller. IEEE Transactions on Automation Science and Engineering 14, 1778–1785. doi:10.1109/TASE.2017.2698923.

Kang, H.H., Lee, D.S., Lim, J.S., Lee, S.J., Jang, J., Jung, K.H., Lee, J., 2021. A study on the effectiveness of the heading control on the mooring line tension and position offset for an arctic floating structure under complex environmental loads. Journal of Marine Science and Engineering 9. doi:10.3390/jmse9020102.

Kjerstad, Ø., Skjetne, R., 2014. Modeling and control for dynamic positioned marine vessels in drifting managed sea ice. Modeling, Identification and Control 35, 249–262. doi:10.4173/mic.2014.4.3.

Kjerstad, Ø.K., Skjetne, R., Jenssen, N.A., 2011. Disturbance rejection by acceleration feedforward: Application to dynamic positioning. IFAC Proceedings Volumes .

Kjerstad, Ø.K., Værnø, S.A.T., Skjetne, R., 2016. A robust dynamic positioning tracking control law mitigating integral windup. IFAC-PapersOnLine 49, 239–244. doi:https://doi.org/10.1016/j.ifacol.2016.10.349.

Lee, J., Choi, S.M., Lee, S.J., Jung, K.H., 2019. Tension based heading control strategy of the arctic fpso with dp assisted mooring system, in: ASME 2019 38th International Conference on Ocean, Offshore and Arctic Engineering, Glasgow, Scotland, UK. pp. 1–7. doi:10.1115/omae2019-96557.

Li, G., 2012. Arctic fpso: Technical feasibilities and challenges, in: ASME 2012 31st International Conference on Ocean, Offshore and Arctic Engineering, American Society of Mechanical Engineers. pp. 379–385.

Mååttånen, M., Kårnå, T., 2011. Iso 19906 ice crushing load design extension for narrow structures, in: Proceedings of the International Conference on Port and Ocean Engineering Under Arctic Conditions, pp. 197–203.

Madsen, H.O., Krenk, S., Lind, N., 2006. Methods of structural safety. Dover Publications, Mineola, New York.

Ngongi, W.E., Du, J.L., 2014. A high-gain observer-based pd controller design for dynamic positioning of ships. Applied Mechanics and Materials 490-491, 803–808. doi:10.4028/www.scientific.net/AMM.490-491.803.

Nguyen, D.T., Sørensen, A.J., 2009a. Setpoint chasing for thruster-assisted position mooring. IEEE Journal of Oceanic Engineering 34, 548–558. doi:10.1109/JOE.2009.2034553.

Nguyen, D.T., Sørensen, A.J., 2009b. Switching control for thruster-assisted position mooring. Control Engineering Practice 17, 985–994.

Rahimi, M., Rausand, M., Wu, S., 2011. Reliability prediction of offshore oil and gas equipment for use in an arctic environment, in: 2011 International Conference on Quality, Reliability, Risk, Maintenance, and Safety Engineering, pp. 81–86. doi:10.1109/ICQR2MSE.2011.5976574.

Sangsoo, R., Kim, M.H., 2003. Coupled dynamic analysis of thruster-assisted turret-moored fpso, in: Oceans 2003. Celebrating the Past ... Teaming Toward the Future, pp. 1613–1620 Vol.3.

Sinsabvarodom, C., Leira, B.J., Chai, W., Næss, A., 2021. Short-term extreme mooring loads prediction and fatigue damage evaluation for station-keeping trials in ice. Ocean Engineering 242, 109930. doi:https://doi.org/10.1016/j.oceaneng.2021.109930.

Skjetne, R., Ren, Z.R., 2020. A survey on modeling and control of thruster-assisted position mooring systems. Marine Structures 74.

Slotine, J.J.E., Li, W., et al., 1991. Applied nonlinear control. volume 199. Prentice hall Englewood Cliffs, NJ.

Sørensen, A.J., 2005. Marine cybernetics: Modelling and control. Lecture Notes, Fifth Edition, UK-05-76, Department of Marine Technology, the Norwegian University of Secience and Technology, Trondheim, Norway .

Strand, J.P., Sørensen, A.J., Fossen, T.I., 1998. Design of automatic thruster assisted mooring systems for ships. Modeling, Identification and Control (MIC) MIC-19.

Su, B., Riska, K., Moan, T., 2010. A numerical method for the prediction of ship performance in level ice. Cold Regions Science and Technology 60, 177–188.

Tuo, Y., Wang, Y., Yang, S.X., Biglarbegian, M., Fu, M., 2018. Robust adaptive dynamic surface control based on structural reliability for a turret-moored floating production storage and offloading vessel. International Journal of Control Automation and Systems 16, 1648–1659. doi:10.1007/s12555-017-0492-5.

Wang, F., Wang, J.m., Wang, K., Zong, Q., Hua, C., 2021. Adaptive backstepping sliding mode control of uncertain semi-strict nonlinear systems and application to permanent magnet synchronous motor. Journal of Systems Science and Complexity 34, 552–571. doi:10.1007/s11424-020-9132-x.

Wang, L., Yang, J., He, H., Xu, S., Su, T.C., 2016. Numerical and experimental study on the influence of the set point on the operation of a thruster-assisted position mooring system. International Journal of Offshore and Polar Engineering 26, 423–432.

Wang, L.X., 1999. A course in fuzzy systems. Prentice-Hall press, USA.

Wang, Y., Tuo, Y., Yang, S.X., Biglarbegian, M., Fu, M., 2018. Reliability-based robust dynamic positioning for a turret-moored floating production storage and offloading vessel with unknown time-varying disturbances and input saturation. Isa Transactions 78, 66–79. doi:10.1016/j.isatra.2017.12.023.

Wu, G., Kong, S., Tang, W., Lei, R., Ji, S., 2021. Statistical analysis of ice loads on ship hull measured during arctic navigations. Ocean Engineering 223, 108642.

Xia, G., Liu, C., Zhao, B., Chen, X., Shao, X., 2019. Finite time output feedback control for ship dynamic positioning assisted mooring positioning system with disturbances. International Journal of Control, Automation and Systems 17, 2948–2960. doi:10.1007/s12555-019-0023-7.

Yu, S., Wang, L., Li, B., He, H., 2020. Optimal setpoint learning of a thruster-assisted position mooring system using a deep deterministic policy gradient approach. Journal of Marine Science and Technology 25, 757–768.

Zhou, L., Moan, T., Riska, K., Su, B., 2013. Heading control for turret-moored vessel in level ice based on kalman filter with thrust allocation. Journal of Marine Science and Technology 18, 460–470.

Zhou, L., Su, B., Riska, K., Moan, T., 2011. Numerical simulation of moored ship in level ice, in: ASME 2011 30th International Conference on Ocean, Offshore and Arctic Engineering, pp. 855–863.

Xiaoyue Zhang received a B.S. from Harbin Institute of Technology. She is currently a Ph.D. student with the College of Intelligent Systems Science and Engineering in Harbin Engineering University, Harbin, China. Her research interests include surface ship control, dynamic positioning system research and position mooring control.

Yuanhui Wang received a B.S., M.S. and Ph.D. from Harbin Engineering University. She is currently a Professor with the College of Intelligent Systems Science and Engineering in Harbin Engineering University, Harbin, China. Her research interests include guidance, navigation and control of marine crafts, autonomy and intelligence of marine robotics, ship dynamic positioning, high-speed ship dynamics and control, robot path planning and signal processing.

Ahmed Chemori received the M.Sc. and Ph.D. degrees both in automatic control from the Grenoble Institute of Technology, Grenoble, France, in 2001 and 2005, respectively. He has been a Postdoctoral Fellow with the Automatic Control Laboratory, Grenoble, France, in 2006. He is currently a tenured Research Scientist in automatic control and robotics with the Montpellier Laboratory of Informatics, Robotics, and Microelectronics. His research interests include nonlinear, adaptive, and predictive control and their applications in robotics.